Effect of Sb in thick InGaAsSbN layers grown by liquid phase epitaxy

V. Donchev[1*] , M. Milanova[2], I. Asenova[1], N. Shtinkov[3], D. Alonso-Álvarez[4], A. Mellor[4], J. Karmakov[1], S. Georgiev[1] and N. Ekins-Daukes[4]

[1] Faculty of Physics, Sofia University, 5, J.Bourchier blvd., Sofia-1164, Bulgaria

[2] Central Laboratory of Applied Physics, 59 St. Petersburg blvd, 4000 Plovdiv, Bulgaria

[3] 510-67 Cartier St., Ottawa, ON, K2P 1J6 Canada

[4] Department of Physics, Imperial College London, London, UK

Keywords:

Abstract

Dilute nitride InGaAsSbN layers grown by low-temperature liquid phase epitaxy are studied in comparison with quaternary InGaAsN layers grown at the same growth conditions to understand the effect of Sb in the compound. The lattice mismatch to the GaAs substrate is found to be slightly larger for the InGaAsNSb layers, which is explained by the large atomic radius of Sb. A reduction of the band gap energy with respect to InGaAsN is demonstrated by means of photoluminescence (PL), surface photovoltage (SPV) spectroscopy and tight-binding calculations. The band-gap energies determined from PL and ellipsometry measurements are in good agreement, while SPV spectroscopy and the tight-binding calculations provide lower values. Possible reasons for these discrepancies are discussed. The PL spectra reveal localized electronic states in the band gap near the conduction band edge, which is confirmed by SPV spectroscopy. The analysis of the power dependence of the integrated PL has allowed determining the dominant recombination mechanisms in the layers. The values of the refraction index in the 450 nm - 1300 nm range are found to be higher for the Sb containing layers.

[*] Corresponding author. E-mail address: vtd@phys.uni-sofia.bg

1. Introduction

Thick layers of dilute nitride InGaAsN and InGaAsSbN grown on GaAs substrate are promising materials for high-efficiency multijunction solar cells applications. Indeed, the current world record triple junction solar cell using the lattice-matched configuration employs InGaAsNSb junction as bottom junction [1] and there is intense work worldwide to extend the application to four junctions. The advantage of InGaAsSbN over InGaAsN is the possibility to achieve longer wavelengths while keeping the structure quasi-lattice matched to GaAs and, more importantly, achieving superior optical and electrical quality. There are many reports on the effects of adding Sb in InGaAsN quantum wells (QWs) and it has been found that InGaAsSbN is a potentially superior material to InGaNAs for long wavelength laser applications [2–6]. It has been proposed that antimony acts as a reactive surfactant, with its atoms segregating on the growth surface and incorporating into the film in only dilute concentrations. The presence of Sb surfactant during molecular beam epitaxy (MBE) growth of dilute nitride semiconductors such as GaAsN dramatically reduces the surface roughness, improves the photoluminescence (PL) efficiency and increases the nitrogen incorporation efficiency [7]. Recently, improved carrier confinement and reduced Auger recombination have been envisaged for dilute nitride lasers based on InGaAsSbN QWs structures on InP substrates [8].

In the context of solar cells, using Sb in either GaAsSbN alloys or InGaAsSbN allows tends to yield better carrier collection properties [9,10]. However, there have been only few reports about the effects of adding Sb in thick InGaAsN layers that are needed for highly efficient solar cells, mostly limited to layers of 1-1.5 μm thickness [11,12]. Similarly to InGaAsN, the InGaAsSbN material has an anomalous band structure due to N-related defects. Many problems related to lattice matching, phase separation, crystal quality, and optical quality

arise during epitaxial growth of the pentanary compounds, together with an increased difficulty in controlling and adjusting the composition [13]. It has been found that the layer properties dramatically depend on growth conditions. High background doping concentrations in MOCVD-grown layers have been obtained due to carbon incorporation [14,15]. Depending on the Sb sources, the background concentration varies in a wide range. Multiple X-ray diffraction (XRD) peaks have been reported for some samples [15], possibly indicating compositional phase separation. It has been found that after thermal annealing the PL intensity vastly increases. In MOCVD-fabricated solar cell structures with a relatively thin (250 nm) 1eV-InGaAsSbN base layer, efficiencies as high as 4.58% have been reported [16].

In MBE grown InGaAsSbN layers the background doping density is significantly lower than that in InGaAsN materials. Solar cell structures based on InGaAsSbN materials have shorter lifetimes as compared to InGaAsN, but higher collection efficiency due to the larger depletion width, caused by lower background doping. The open-circuit voltage is somewhat degraded compared to InGaAsN devices [17]. Using realistic solar cell parameters for double- and triple-junction solar cells, Aho et al. [18] have estimated the efficiency of a four-junction GaInP/GaAs/GaInNAs/Ge solar cell at AM1.5D 1-sun illumination to be over 36%.

In the case of MBE growth of InGaAsSbN on InP substrates it has been found that adding Sb improves the crystallographic quality of the thick dilute nitride layer and the PL peak shifts to longer wavelengths [19]. However, the PL intensity decreases, supposedly due to the influence of the growth conditions [19].

Contrary to MOCVD and MBE the growth by liquid phase epitaxy (LPE) occurs at nearly thermodynamic equilibrium conditions and with higher growth rates. This allows obtaining thick layers of high quality material in terms of lifetime, mobility and freedom from defects, suitable for solar cell applications. In spite of this there have been few reports on Ga(In)AsN layers grown by LPE [20–24] and even fewer for the LPE-grown pentanary compound

InGaAsSbN [25]. Therefore, it is important to study such materials by various complementary experimental techniques. In [25] we have presented initial PL and surface photovoltage (SPV) spectroscopy results obtained in thick InGaAsSbN layers grown by LPE. In the present work we extend our investigations in this field using XRD and spectroscopic ellipsometry, in addition to PL and SPV, together with theoretical calculations to get a deeper understanding of the effect of Sb in thick InGaAsN layers grown by LPE.

2. Experimental details

Dilute nitride epitaxial layers were grown by the horizontal graphite slider-boat technique for LPE on n-type (100) GaAs:Si (~10^{18}cm^{-3}) substrates. No special baking of the system was carried out before epitaxy. The starting materials for the solutions consisted of 6N pure solvent metals Ga, In and Sb. Polycrystalline GaAs and GaN were used as sources of As and N, respectively. The charged boat was annealed at 680°C for 1 h under Pd-diffused ultra-pure hydrogen flow in order to homogenize the melt and to reduce the residual impurities. Two series of samples were grown from mixed solutions with two different compositions: 90%In +10%Ga, and 86%In+10%Ga+4%Sb. The N content in the melt was 0.5 at.% for all samples. The crystallization was carried out from initial epitaxy temperature of 569 ºC for 3 minutes, at a cooling rate of 1 ºC/min.

A LYRA I XMU (Tescan) scanning electron microscope (SEM) equipped with an energy dispersive X-ray (EDX) microanalyzer (Quantax, Bruker) was used to determine the layer thicknesses and composition. The layer thickness was found to be about 2.1-2.3 μm. EDX measurements revealed 3% In concentration in both series of samples and about 0.5% Sb concentration in the InGaAsSbN samples. The content of N was estimated by means of XRD and the content found for In and Sb (see below). Hall measurements revealed n-type doping of the layers in the range 6-7×10^{17}cm^{-3}.

High-resolution XRD was used for determination of the lattice parameter, strain and crystalline quality of the layers. The measurements were performed in the θ/2θ geometry on a Seifert XRD 3003 PTS diffractometer, which utilizes a parallel beam with monochromatic Cu Kα1 radiation (λ = 0.15406 nm, a 2-bounce Ge (220) crystal primary monochromator) and a scintillation detector.

Photoluminescence experiments used a Millenia V neodymium yttrium vanadate ($NdYVO_4$) laser emitting at 532 nm as excitation source. Light emitted by the samples was dispersed with a 0.5 m focal length spectrometer (Acton 2300i, Princeton Instruments) and detected with a Si photodiode. All PL measurements were performed at room temperature.

SPV spectra were recorded at room temperature applying the metal-insulator-semiconductor operation mode of the SPV technique [26]. Details about the SPV experimental set-up and measurement procedure can be found in [27]. The probe electrode was a semitransparent SnO_2 film evaporated on the bottom surface of a quartz glass separated from the sample by a 15-μm thick mica sheet. The sample was illuminated by a 250 W halogen lamp along with a grating monochromator. The light was chopped at 94 Hz and the photon flux was kept constant ($\approx 1.5\times10^{14}$ $cm^{-2}s^{-1}$) for all wavelengths. Special care was taken to eliminate any effect on the measured SPV phase resulting from the electrical measurement circuit and from the reference signal of the optical chopper [27].

Spectroscopic ellipsometry measurements were carried out by means of a Woollam variable angle spectroscopic ellipsometer. The ellipsometric angles ψ and Δ were measured in the range from 260 to1300 nm at incident angles of 65, 70 and 75 degrees.

3. Theoretical calculations

The band structures of InGaAs(Sb)N compounds were calculated using a semi-empirical $sp^3d^5s^*s_N$ tight-binding model, including spin [28]. The N-related parameters have shown a

negligible dependence on the host material [28,29], therefore we have used for both the quaternary and the pentanary compounds the parameters from Ref. [28]. Band offsets, lattice constants, and other material parameters were taken from Ref. [30]. For calculating lattice-matched concentrations, the lattice constant of the alloys was assumed to depend linearly on the lattice constants of the binaries (Vegard's rule) [30]. Although in dilute nitrides many parameters have non-linear dependencies on concentration, the lattice constant generally follows Vegard's rule; deviations have been shown to arise under specific growth conditions far from equilibrium [31].

The model parameters were carefully chosen to reproduce precisely the band structures of pure III-V binaries, alloys and dilute nitride compounds at low temperatures (~2K) [28,29]. To compare to room temperature measurements, a temperature correction was applied. In the absence of N, the properties of III-V alloys vary quasi-linearly depending on the alloy composition; thus, one can reasonably assume that the low (< 3%) Sb and In concentrations do not affect significantly the temperature dependence of the band gap. Therefore, we used the temperature correction (band gap difference between 2 K and 300 K) for dilute $GaAs_{1-x}N_x$, which varies linearly from 100 meV for $x = 0$ to 70 meV for $x = 0.5\%$ [32].

4. Results and Discussion

4.1. XRD

Typical HRXRD (004) scan spectra of InGaAsN and InGaAsSbN epilayers are displayed on figure 1. The analysis of the spectra has shown that better lattice matching is achieved for the quaternary InGaAsN layers - the lattice mismatch $\Delta a/a_o$ is 0.20% and 0.16% for the samples with and without Sb. This is in accordance with the large atomic radius of Sb. From the above depicted values and the contents of In and Sb, the content of N is determined by means of Vegard's rule [2,30] and the value 0.27 % is obtained for both types of samples. The use of

Vegard's rule in the present case is justified by the low concentrations of In, Sb and N [31,33]. There is a shoulder in the InGaAsSbN related peak, which can be due to a local relaxation or local deviation from the chemical composition.

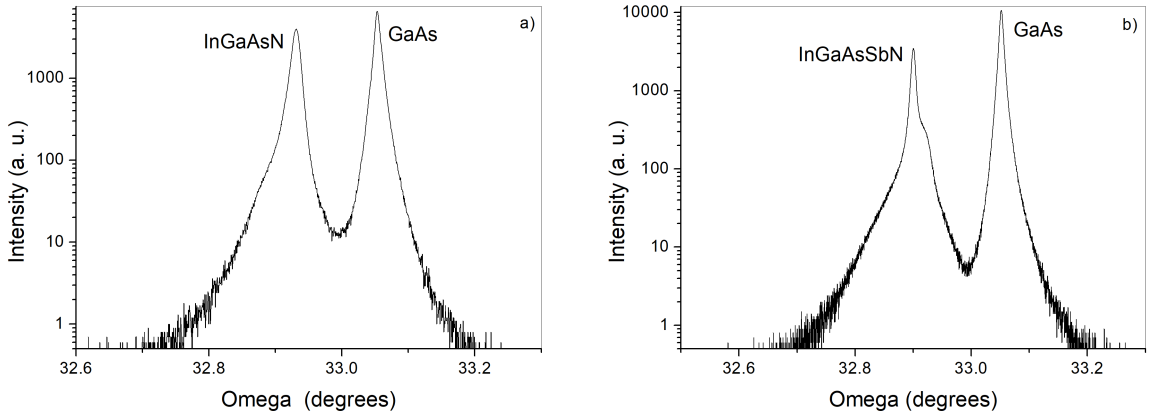

Figure 1. High-resolution X-ray diffraction (004) curves for (a) InGaAsN and (b) InGaAsSbN samples

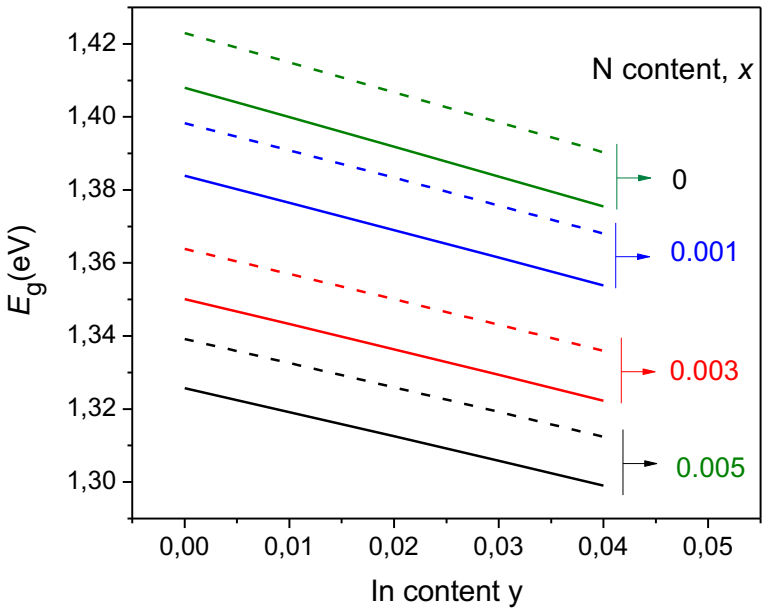

Figure 2. Calculated bandgap energy of $In_yGa_{1-y}As_{1-x-z}Sb_zN_x$ as a function of the In content, for Sb concentrations of 0.5% (solid lines) and 0% (dotted lines). Curves of different colours correspond to different N fractions as shown.

Theoretical calculations

Figure 2 shows the calculated dependences of the $In_yGa_{1-y}As_{1-x-z}Sb_zN_x$ band gap in the expected range of N, In, and Sb concentrations. The addition of Sb reduces the bandgap by 13-15 meV. The band gaps corresponding to the experimentally found In content of 0.03 and N content of 0.0027 are 1.348 eV for the case without Sb and 1.334 eV for the case of 0.5% Sb.

4.2. Photoluminescence spectroscopy

Figure 3 presents room temperature PL spectra of an InGaAsN and an InGaAsSbN layers grown at the same growth conditions. In both cases, the spectrum reveals a relatively broad peak interpreted as band-edge luminescence. An exponential tail is present at the high-energy side of the peak resulting from the Boltzmann carrier distribution. Similar exponential component is observed at the low energy side and attributed to an extended distribution of localised states within the band gap (Urbach's tail). As can be seen from figure 3, for the given In and N contents, the band gap energy decreases with adding Sb by 11 meV. Contrary to GaAsN and InGaAsN, the band gap evolution of As-rich GaAsSb is mainly due to the increase of the valence band maximum with increasing Sb content. It is known that the band gap decreases linearly with the Sb concentration, changing by ≈20 meV/at. % for both pure ternary GaAsSb [34] and dilute nitride GaAsSbN [35]. For InGaAsSbN the band gap evolution is more complex than those of dilute nitride (In)GaAsN and antimonide GaAsSb compounds and so far its exact physical mechanism is still unclear. The band gap energy dependence on Sb and In contents is very similar to the composition dependence of the band gap energy of the conventional semiconductor alloys (without N). On the other hand, the band gap energy dependence on N content shows a large band gap bowing, since the coupling between the N level and the conduction band minimum of the host material is stronger than the effects of Sb

and In. Based on the above we conclude that the band gap shift with respect to GaAs for the InGaAsSbN sample is mainly due to the effect of N with a weaker but not negligible contribution from the effect of Sb.

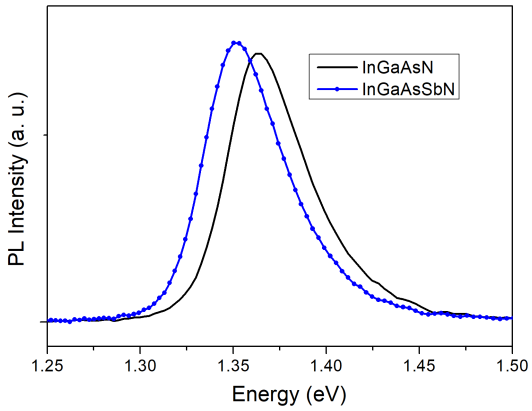

Figure 3. Room temperature PL spectra of InGaAsN and InGaAsSbN samples grown at the same growth conditions

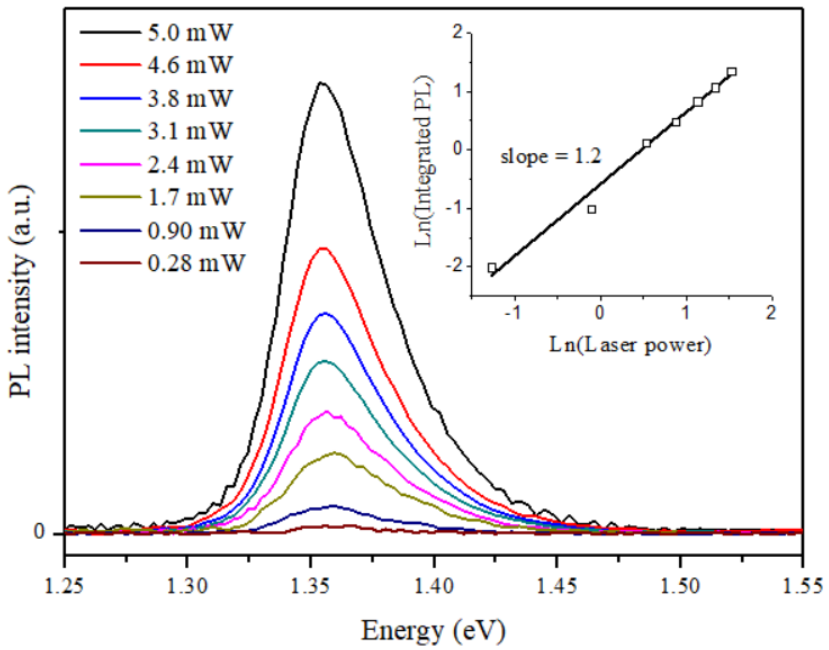

Figure 4. PL spectra of an InGaAsSbN sample at different laser excitation powers. The inset shows the dependence of the integrated PL intensity on the laser power.

Figure 4 displays PL spectra recorded in one of the InGaAsSbN samples at various excitation densities ranging from 0.28 mW to 5 mW. The luminescence intensity increases with excitation density and no shift of the PL peak position of the band-edge luminescence is observed. The inset shows the integrated PL intensity as a function of the laser power in double logarithmic scale. The dependence of the integrated PL, I_{PL}, in semiconductor materials on the light excitation density, I_{exc}, is usually represented as a power function $I_{PL} \sim I_{exc}^{k}$ and has been discussed in the literature together with different proposed models [36,37]. For example in the model from [36], developed for low temperature PL, the power coefficient is $1 < k < 2$ for free- and bound-exciton emission, while k is less than 1 for free-to-bound and donor-acceptor pair recombination. No free carrier recombination is considered. In [37] a model is proposed for room temperature PL of GaAs/AlGaAs multiple quantum wells, which leads to $k = 1$ for free exciton recombination and $k = 2$ for free carrier bimolecular recombination. This model assumes negligible equilibrium carrier densities and domination of non-radiative recombination. For dilute nitride alloys the integrated PL intensity has been studied as a function of the temperature [38,39], but we could not find studies on its excitation density dependence. Therefore to discuss this dependence in our case we use the model from [37], which is for room temperature PL. We however take into account that the equilibrium electron concentration n_0 is of the order of $6\text{-}7\times10^{17}\text{cm}^{-3}$, while the excess concentration of electrons Δn and holes Δp at the maximum applied laser power are assessed to be more than two orders of magnitude lower. The PL emission is given by $B(n_0+\Delta n)\Delta p$, where B is the radiative recombination rate in cm^3s^{-1}, and $\Delta n << n_0$. If one neglect in a first approximation Δn, the emission term becomes $Bn_0\Delta p$ and its dependence on the light excitation density only comes from Δp, which is proportional to I_{exc}. Therefore one should expect $k = 1$ in the dependence $I_{PL} \sim I_{exc}^{k}$. The inset of figure 4 shows that $k = 1.2$. The values obtained in other samples vary between 1 and 1.2. From these results and the discussion given above, we conclude that in our

samples the dominant recombination mechanisms are free carrier recombination and exciton recombination. The exciton recombination should mainly include excitons localized in potential fluctuations.

The band gap energies obtained from the PL peak positions in different Sb containing samples are higher by some 23 – 25 meV as compared to the calculated values from the simulations. This discrepancy could be due to several factors. The calculations were made for a random alloy using the virtual crystal approximation for the tight-binding parameters of the InGaAsSb quaternary compound. On the other hand Kim and Zunger [40] have shown that the band gap formation of the quaternary InGaAsN depends not only from the composition, but also from the short range ordering of the atoms. The main results of this local ordering are reducing the optical bowing as compared to random alloys case and the appearance of a tail of localized states around the conduction band minimum due to different clusters of nitrogen atoms surrounded by varying number of indium and gallium atoms. This analysis was experimentally confirmed in our recent paper devoted to InGaAsN [41]. Similar short-range ordering probably occurs also in pentanary InGaAsSbN, and could be favoured by the LPE growth at nearly equilibrium conditions, thus increasing the band gap with respect to the random alloy case. Other factors that could affect the accuracy of the simulation results are the uncertainty in determining the temperature dependency of the band gap (partly due to neglecting the In and Sb contributions), the presence of residual strain in the samples, the uncertainties in the experimentally determined composition of the alloy, etc.

4.3. Surface photovoltage spectroscopy

Figure 5a represents the normalized SPV amplitude spectrum of an InGaAsSbN sample compared with that of the GaAs substrate. A clear red shift of the absorption edge is observed for the InGaAsSbN sample with respect to the GaAs substrate. To assess the band gap of the

InGaAsSbN layer we plot the square of the SPV amplitude vs the photon energy, which for the ideal case of a bulk semiconductor should give a straight line resulting from the shape of the 3D joint density of states. In the present case, we consider the linear part of the obtained curve and extrapolate the straight line to find its x-intercept, which is assumed to be the band gap, E_g. For the current sample E_g = 1.324 eV and therefore the band gap shift ΔE_g with respect to GaAs (E_g=1.423 eV) is 99 meV. The same result (within the experimental error) is obtained by using Tauc plot assuming that SPV is proportional to the absorption coefficient. On the other hand, the PL peak for this sample is at 1.357 eV, i.e. at higher energy. Different samples were studied and the band gap shift ΔE_g with respect to GaAs varies between 97 and 112 meV. These values are higher than the ones obtained in LPE grown quaternary InGaAsN layers [25,41]. For all samples the band gap values determined from SPV measurements are lower as compared to those estimated from the PL peak position by some 32 - 49 meV depending on the sample.

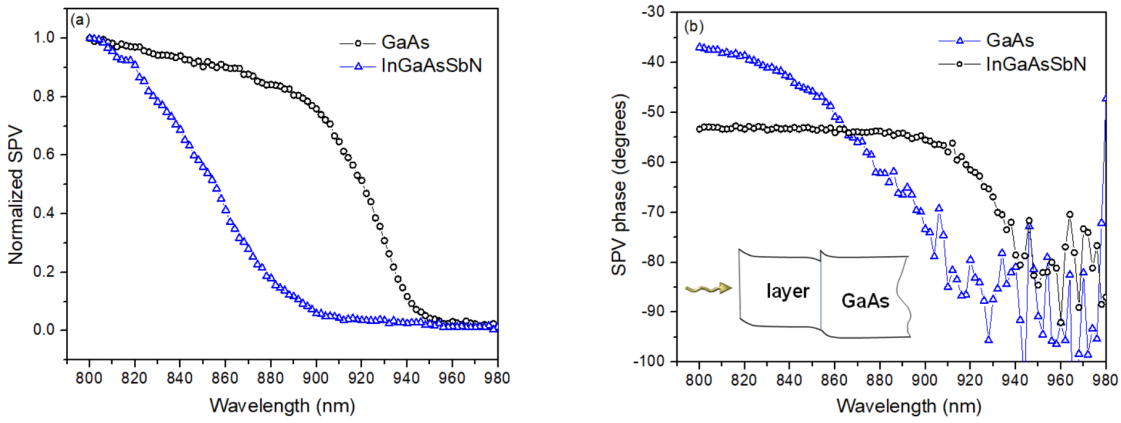

Figure 5. SPV amplitude (a) and phase (b) spectra of an InGaAsSbN sample (circles) and the GaAs substrate (triangles). The inset in (b) schematically shows the energy band alignment in the structure.

Other authors have also reported discrepancies between the band gap values of dilute nitrides estimated from absorption (or SPV) and PL. For example Bansal et al. [42] observed a

Stokes shift between the SPV and PL determined band gaps of $In_yGa_{1-y}As_{1-x}N_x$ samples with y = 0.72 and x ranging from 0.009 to 0.017. Volovik et al. [43] reported that the relation between the band gap values of GaAsN determined from absorption and from PL depends on the N content and the temperature. In particular they observed that for low N content (0.6%) the temperature dependences of the PL peak position and the absorption edge cross at a certain temperature and at 300 K the PL peak is at higher energy than the absorption edge energy. This was explained by thermal emission of carriers from localized states with increasing temperature and dominance of inter-band recombination at 300 K. Such "anti-Stokes" shift between absorption (SPV) and emission is observed also in our samples as stated above.

A tentative explanation of the observed discrepancies between the band gap energies obtained from SPV and PL results is presented below. It is well known that the N atoms in dilute nitrides give origin of a series of defect states, some of which are in the band gap [20,21,40]. The light intensity in the SPV experiment is much lower than that in the PL one. With increasing photon energy, SPV probes first the defect states in the band gap near the conduction band and as a result gives a relatively low optical transition energy. On the other hand, under laser excitation, which is the case of the PL experiment, the defect states are quickly filled with electrons. It is reasonable to assume that these states are slower with respect to recombination (e.g because the electron has to overcome an energy barrier before recombination) than the extended states in the conduction band. This, together with the room temperature, facilitates the thermal emission from these states towards the conduction band. Thus, the PL mainly probes states in the band (i.e. with higher energies), which are faster and more effective for emission. Therefore, the PL peak appears at higher energy than the band gap determined from SPV. The existence of a tail of defect states below the conduction band edge was evidenced in our previous papers on InGaAsN layers by the low-energy tail of the PL spectrum measured at 2K [24,25,41].

Figure 5b shows the SPV phase spectra of the InGaAsSbN sample and the GaAs substrate. From them information about the alignment of the energy bands across the structure can be obtained as follows. The phase values are in the IV quadrant and their spectral behaviour is typical for the case of upwards energy band bending in the direction towards the surface [27]. This indicates and an n-type doping of the layers, in accordance with the Hall measurements results and with our previous results on InGaAsN layers [24]. In addition, the phase values of the InGaAsSbN layer suggest that the energy band bending at the interface layer/substrate is also upwards. This is expected from the fact that under conditions without electrical contact between layer and substrate the Fermi level in the substrate is at higher energy than the one in the layer. At electrical contact electrons flows from the substrate towards the layer, which results in upwards band bending at the interface. The energy band alignment in the structure is schematically shown in the inset of figure 5b.

4.4. Spectroscopic ellipsometry

For the interpretation of the spectroscopic ellipsometric data, a three-layer model is used including a thin native-oxide, unknown layer of InGaAsN or InGaAsSbN alloy and GaAs substrate. The thickness of the native-oxide layer on the front sample surface is fitted to be in range of 3 - 5 nm. The thicknesses of the alloy layers are estimated by means of SEM and EDX as stated above. These thicknesses are used in the fitting model to estimate the refractive index, n, and the extinction coefficient, k of the dilute nitride layers. The refraction index and extinction coefficient of an InGaAsSbN sample in the wavelength range from 250 nm to 1300 nm, are presented in figure 6.

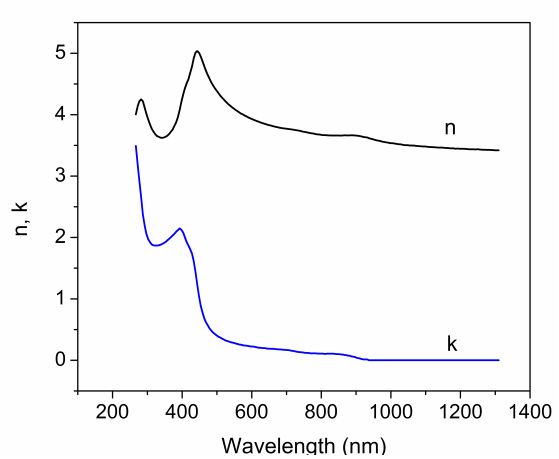

Figure 6. Refraction index *n* and extinction coefficient *k* of an InGaAsSbN layer nearly lattice matched to GaAs substrate.

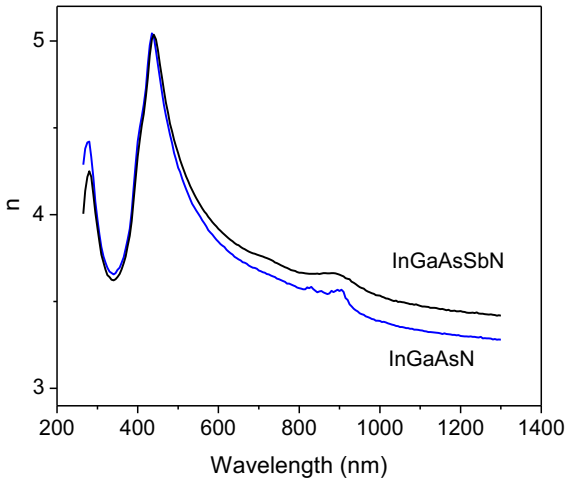

Figure 7. Refractive index of InGaAsN and InGaAsNSb layers nearly lattice matched to GaAs substrate.

To investigate the variation of the refractive index caused by the addition of Sb we compare on figure 7 the spectra of an InGaAsN and an InGaAsNSb layers, which are nearly lattice matched to the GaAs substrate. Although the values are close, it is clearly seen that the *n*-values of the layer containing Sb are higher, the difference increasing with increasing

wavelength from 450 nm to 1300 nm. This finding is in accordance with its lower band gap value. We do not exclude possible influence of differences in the surface quality or artefacts in the fitting process. Nevertheless, this is an intriguing finding since a large refractive index of the alloys represents a significant advantage for the fabrication of high-performance optoelectronic devices [44]. The effect of Sb on the band structure of the alloy is largely limited on the valence band states, while N affects mainly conduction-band states; however the latter has been shown to also have a non-negligible effect on the valence band of the host material even in dilute concentrations [45]. Interactions between the valence band perturbations caused by N and Sb could represent one possible mechanism leading to changes in the refractive index and optical properties of the alloy; however further studies are needed in order to understand these effects.

The absorption coefficient α of the InGaAsSbN laeyr is calculated from the extinction coefficient *k*. The band gap is estimated from the plot of α^2 vs. photon energy $h\nu$ by considering the linear part of the obtained curve and extrapolating the straight line to find its intersection with the abscissa. The same result is obtained by using a Tauc plot, i.e. $(\alpha * h\nu)^2$ vs. $h\nu$ as shown on figure 8. The obtained value is 1.357 eV. It coincides with the PL peak position 1.357 eV of the same sample indicating a good agreement between the two techniques.

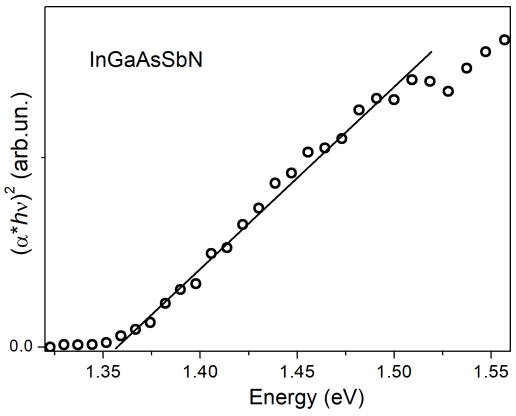

Figure 8. Tauc plot for the InGaAsSbN sample from figure 6.

5. Conclusion

Dilute nitride InGaAsNSb layers nearly lattice matched to GaAs are grown by low-temperature LPE. The properties of the layers are investigated in comparison with those of quaternary InGaAsN layers grown at the same growth conditions. The lattice mismatch to the GaAs substrate is a bit larger for the InGaAsNSb layers, which is in accordance with the large atomic radius of Sb. By means of PL, SPV and tight-binding calculations it is evidenced that the band gap shift with respect to GaAs is larger in the case of the pentanary InGaAsNSb compound. The band gap reduction resulting from Sb incorporation is due to independently controlled increase of the valence band maximum. The band-gap energies determined from PL and variable angle ellipsometry measurements are in good agreement, while SPV spectroscopy and the tight-binding calculations give smaller values by 32 - 49 meV and 23 - 25 meV, respectively depending on the sample. In the case of SPV, the discrepancy is explained by electronic transitions to localized states near the conduction band minimum followed by thermal excitation of electrons to the continuum to contribute to the SPV signal. Short-range ordering favoured by the LPE growth at nearly equilibrium conditions increases the band gap with respect to the random alloy case considered in the tight-binding calculations.

The study of the integrated PL intensity as a function of the excitation power has revealed that free carrier recombination is the dominant recombination mechanism together with localized exciton recombination. The values of the refraction index and the extinction coefficient have been obtained by variable angle spectroscopic ellipsometry for a range of wavelengths from 250 nm to 1300 nm. Higher values of the refractive index are found for Sb containing layers, which can be an advantage for optoelectronic device design and fabrication.

The present study contributes to a better interpretation of the experimental results obtained in LPE grown InGaAsNSb dilute nitrides and better understanding of their properties.

Acknowledgements

This work was supported by the Cost Action MP1406 "Multiscale in modelling and validation for solar photovoltaics (MultiscaleSolar)" and the Bulgarian National Science Fund (contract ДКОСТ 01/16). The authors acknowledge A. Tsonev and K. Genkov for the EDX and SEM measurements, J. W. Gerlach for the XRD data, and B. Arnaudov for the Hall effect measurements.

References

D. Derkacs, R. Jones-Albertus, F. Suarez, O. Fidaner, Lattice-matched multijunction solar cells employing a 1 eV GaInNAsSb bottom cell, J. Photonics Energy. 2 (2012) 21805-1–9. doi:10.1117/1.JPE.2.021805.

[2] J.S. Misiewicz, J., Kudrawiec, R., Gladysiewicz, M., Harris, Electromodulation Spectroscopy of GaInNAsSb/GaAs Quantum Wells: The Conduction Band Offset and the Electron Effective Mass Issues, in: A. Erol (Ed.), Dilute III-V Nitride Semicond. Mater. Syst., Springer, Berlin Heidelberg, 2008: pp. 163–180.

[3] R.A. Arif, N. Tansu, Interdiffused SbN-based Quantum Well on GaAs for 1300-1550 nm Diode Lasers, MRS Proc. 891 (2005). doi:DOI: 10.1557/PROC-0891-EE11-09.

[4] Y. Kawamura, M. Nishino, Effect of Sb Incorporation on Electroluminescence of InGaAsSbN Quantum Well Diodes Grown on GaAs Substrates, Jpn. J. Appl. Phys. 47 (2008) 6302–6303. doi:10.1143/JJAP.47.6302.

[5] J.S. Bank, S.R., Bae, H.P., Yuen, H.B., Wistey, M.A., Goddard, L.L., Harris, Room-temperature continuous-wave 1.55 μm GaInNAsSb laser on GaAs, Electron. Lett. 42 (2006) 156–157. http://digital-library.theiet.org/content/journals/10.1049/el_20064022 (accessed April 4, 2017).

[6] J.S.Harris, GaInNAs and GaInNAsSb Long-Wavelength Lasers, in: I. A. Buyanova and W. M. Chen (Ed.), Phys. Appl. Dilute Nitrides, Taylor and, Taylor & Francis, New York, 2004: pp. 395–433.

[7] J.S.Harris, GaInNAs and GaInNAsSb Long-Wavelength Lasers, in: I. A. Buyanova and W. M. Chen (Ed.), Phys. Appl. Dilute Nitrides, Taylor & Francis, New York, 2004: pp. 395–433.

[8] Y. Kawamura, InP-based InGaAsSbN quantum well laser diodes in the 2-μm wavelength region, Electron. Commun. Japan. 94 (2011) 33–38. doi:10.1002/ecj.10195.

[9] T. Thomas, M. Fuhrer, D.A. Alvarez, N. Ekins-Daukes, K.H. Tan, S. Wicaksono, W.K. Loke, S.F. Yoon, A. Johnson, GaNAsSb 1-eV solar cells for use in lattice-matched multi-junction architectures, in: 2014 IEEE 40th Photovolt. Spec. Conf., IEEE, 2014: pp. 0550–0553. doi:10.1109/PVSC.2014.6924980.

[10] D.B. Jackrel, S.R. Bank, H.B. Yuen, M.A. Wistey, J.S. Harris, A.J. Ptak, S.W. Johnston, D.J. Friedman, S.R. Kurtz, Dilute nitride GaInNAs and GaInNAsSb solar cells by molecular beam epitaxy, J. Appl. Phys. 101 (2007) 114916. doi:10.1063/1.2744490.

[11] S.L. Tan, W.M. Soong, M.J. Steer, S. Zhang, J.S. Ng, J.P.R. David, Dilute nitride GaInNAs and GaInNAsSb for solar cell applications, in: A. Freundlich, J.-F.F. Guillemoles (Eds.), 2012: p. 82561E. doi:10.1117/12.910349.

[12] A. Gubanov, V. Polojärvi, A. Aho, A. Tukiainen, N. V Tkachenko, M. Guina, Dynamics of time-resolved photoluminescence in GaInNAs and GaNAsSb solar cells., Nanoscale Res. Lett. 9 (2014) 80. doi:10.1186/1556-276X-9-80.

[13] A. Aho, V.-M. Korpijärvi, R. Isoaho, P. Malinen, A. Tukiainen, M. Honkanen, M.

Guina, Determination of composition and energy gaps of GaInNAsSb layers grown by MBE, J. Cryst. Growth. 438 (2016) 49–54. doi:10.1016/j.jcrysgro.2015.12.026.

[14] T.W. Kim, T.J. Garrod, L.J. Mawst, T.F. Kuech, S.D. LaLumondiere, Y. Sin, W.T. Lotshaw, S.C. Moss, Characteristics of bulk InGaAsSbN/GaAs grown by metalorganic vapor phase epitaxy (MOVPE), J. Cryst. Growth. (2013). doi:10.1016/j.jcrysgro.2012.06.043.

[15] T. Kim, T.J. Garrod, K. Kim, J. Lee, L.J. Mawst, T.F. Kuech, S.D. LaLumondiere, Y. Sin, W.T. Lotshaw, S.C. Moss, Characteristics of bulk InGaAsN and InGaAsSbN material grown by metal organic vapor phase epitaxy (MOVPE) for solar cell application, in: A. Freundlich, J.-F.F. Guillemoles (Eds.), International Society for Optics and Photonics, 2012: p. 82561D. doi:10.1117/12.906961.

[16] T.W. Kim, T.J. Garrod, K. Kim, J.J. Lee, S.D. Lalumondiere, Y. Sin, W.T. Lotshaw, S.C. Moss, T.F. Kuech, R. Tatavarti, L.J. Mawst, Narrow band gap (1 eV) InGaAsSbN solar cells grown by metalorganic vapor phase epitaxy, Appl. Phys. Lett. 100 (2012) 13–17. doi:10.1063/1.3693160.

[17] D.B. Jackrel, S.R. Bank, H.B. Yuen, M.A. Wistey, J.S. Harris, A.J. Ptak, S.W. Johnston, D.J. Friedman, S.R. Kurtz, Dilute nitride GaInNAs and GaInNAsSb solar cells by molecular beam epitaxy, J. Appl. Phys. 101 (2007) 114916. doi:10.1063/1.2744490.

[18] A. Aho, A. Tukiainen, V. Polojärvi, M. Guina, Performance assessment of multijunction solar cells incorporating GaInNAsSb, Nanoscale Res. Lett. 9 (2014) 61. doi:10.1186/1556-276X-9-61.

[19] K. Miura, Y. Nagai, Y. Iguchi, H. Okada, Y. Kawamura, Improvement of crystal quality of thick InGaAsN layers grown on InP substrates by adding antimony, J. Cryst.

Growth. 301 (2007) 575–578. doi:10.1016/j.jcrysgro.2006.11.154.

[20] S. Bhuyan, S.K. Das, S. Dhar, B. Pal, B. Bansal, Optical density of states in ultradilute GaAsN alloy: Coexistence of free excitons and impurity band of localized and delocalized states, J. Appl. Phys. 116 (2014) 23103. doi:10.1063/1.4886178.

[21] S. Dhar, N. Halder, A. Mondal, B. Bansal, B.M. Arora, Detailed studies on the origin of nitrogen-related electron traps in dilute GaAsN layers grown by liquid phase epitaxy, Semicond. Sci. Technol. 20 (2005) 1168–1172. doi:10.1088/0268-1242/20/12/004.

[22] M. Milanova, P. Vitanov, P. Terziyska, G. Popov, G. Koleva, Structural and electrical characteristics of InGaAsN layers grown by LPE, J. Cryst. Growth. 346 (2012) 79–82. doi:10.1016/j.jcrysgro.2012.02.021.

[23] M. Milanova, P. Vitanov, P. Terziyska, G. Koleva, G. Popov, Nitrogen incorporation into GaAsN and InGaAsN layers grown by liquid-phase epitaxy, Phys. Status Solidi Curr. Top. Solid State Phys. 10 (2013) 597–600. doi:10.1002/pssc.201200890.

[24] V. Donchev, M. Milanova, J. Lemieux, N. Shtinkov, I.G. Ivanov, Surface photovoltage and photoluminescence study of thick Ga(In)AsN layers grown by liquid-phase epitaxy, J. Phys. Conf. Ser. 700 (2016) 12028. doi:10.1088/1742-6596/700/1/012028.

[25] V. Donchev, I. Asenova, M. Milanova, D.A. Alvarez, K. Kirilov, N. Shtinkov, I.G. Ivanov, S. Georgiev, E. Valcheva, N. Ekins-Daukes, Optical properties of thick GaInAs (Sb) N layers grown by liquid-phase epitaxy, J. Phys. Conf. Ser. 794 (2017) 12013.

[26] L. Kronik, Y. Shapira, Surface photovoltage phenomena: Theory, experiment, and applications, Surf. Sci. Rep. 37 (1999) 1–206. doi:10.1016/S0167-5729(99)00002-3.

[27] V. Donchev, T. Ivanov, K. Germanova, K. Kirilov, Surface photovoltage spectroscopy

– an advanced method for characterization of semiconductor nanostructures, Trends Appl. Spectrosc. 8 (2010) 27–66.

[28] N. Shtinkov, P. Desjardins, R. Masut, Empirical tight-binding model for the electronic structure of dilute GaNAs alloys, Phys. Rev. B. 67 (2003) 81202. doi:10.1103/PhysRevB.67.081202.

[29] S. Turcotte, N. Shtinkov, P. Desjardins, R.A. Masut, R. Leonelli, Empirical tight-binding calculations of the electronic structure of dilute III–V–N semiconductor alloys, J. Vac. Sci. Technol. A Vacuum, Surfaces, Film. 22 (2004) 776. doi:10.1116/1.1688361.

[30] I. Vurgaftman, J.R. Meyer, L.R. Ram-Mohan, Band parameters for III–V compound semiconductors and their alloys, J. Appl. Phys. 89 (2001) 5815.

[31] N. Shtinkov, P. Desjardins, R. Masut, M. Côté, Nitrogen incorporation and lattice constant of strained dilute $GaAs_{1-x}N_x$ layers on GaAs (001): An ab initio study, Phys. Rev. B. 74 (2006) 1–8. doi:10.1103/PhysRevB.74.035211.

[32] K. Uesugi, I. Suemune, T. Hasegawa, T. Akutagawa, T. Nakamura, Temperature dependence of band gap energies of GaAsN alloys, Appl. Phys. Lett. 76 (2000) 1285. doi:10.1063/1.126010.

[33] Y.K. Kuo, B.T. Liou, S.H. Yen, H.Y. Chu, Vegard's law deviation in lattice constant and band gap bowing parameter of zincblende $In_xGa_{1-x}N$, Opt. Commun. 237 (2004) 363–369. doi:10.1016/j.optcom.2004.04.012.

[34] L.F. Bian, D.S. Jiang, P.H. Tan, S.L. Lu, B.Q. Sun, L.H. Li, J.C. Harmand, Photoluminescence characteristics of GaAsSbN/GaAs epilayers lattice-matched to GaAs substrates, Solid State Commun. 132 (2004) 707–711. doi:10.1016/j.ssc.2004.09.016.

[35] T.S. Wang, J.T. Tsai, K.I. Lin, J.S. Hwang, H.H. Lin, L.C. Chou, Characterization of band gap in GaAsSb/GaAs heterojunction and band alignment in GaAsSb/GaAs multiple quantum wells, Mater. Sci. Eng. B. 147 (2008) 131–135. doi:10.1016/j.mseb.2007.09.075.

[36] T. Schmidt, K. Lischka, W. Zulehner, Excitation-power dependence of the near-band-edge photoluminescence of semiconductors, Phys. Rev. B. 45 (1992) 8989–8994. doi:10.1103/PhysRevB.45.8989.

[37] J.E. Fouquet, A.E. Siegman, Room- temperature photoluminescence times in a GaAs/Al $_{x}$ Ga $_{1-x}$ As molecular beam epitaxy multiple quantum well structure, Appl. Phys. Lett. 46 (1985) 280–282. doi:10.1063/1.95658.

[38] I.A. Buyanova, M. Izadifard, W.M. Chen, A. Polimeni, M. Capizzi, H.P. Xin, C.W. Tu, Hydrogen-induced improvements in optical quality of GaNAs alloys, Appl. Phys. Lett. 82 (2003) 3662–3664. doi:10.1063/1.1578513.

[39] B. Kuner, D. Trusheim, V. Voßebuvrger, K. Volz, W. Stolz, Annealing experiments of the GaP based dilute nitride Ga(NAsP), Phys. Status Solidi Appl. Mater. Sci. 205 (2008) 114–119. doi:10.1002/pssa.200777476.

[40] K. Kim, A. Zunger, Spatial correlations in GaInAsN alloys and their effects on band-gap enhancement and electron localization, Phys. Rev. Lett. 86 (2001) 2609–2612.

[41] M. Milanova, V. Donchev, K.L. Kostov, D. Alonso-Álvarez, E. Valcheva, K. Kirilov, I. Asenova, I.G. Ivanov, S. Georgiev, N. Ekins-Daukes, Experimental study of the effect of local atomic ordering on the energy band gap of melt grown InGaAsN alloys, Semicond. Sci. Technol. (2017). doi:doi.org/10.1088/1361-6641/aa7404.

[42] B. Bansal, A. Kadir, A. Bhattacharya, B.M. Arora, R. Bhat, Alloy disorder effects on the room temperature optical properties of GaInNAs quantum wells, Appl. Phys. Lett.

89 (2006) 32110. doi:10.1063/1.2227618.

[43] B. V Volovik, N. V Kryzhanovskaya, D.S. Sizov, A.R. Kovsh, A.F. Tsatsul' nikov, J.Y. Chi, J.S. Wang, L. Wei, V.M. Ustinov, Effect of carrier localization on the optical properties of MBE-grown GaAsN/GaAs heterostructures, Semiconductors. 36 (2002) 997–1000. doi:10.1134/1.1507281.

[44] P.-W. Li, H.-C. Guang, N.-Y. Li, Ellipsometric Study of the Optical Properties of InGaAsN Layers, Jpn. J. Appl. Phys. 39 (2000) L898–L900. doi:10.1143/JJAP.39.L898.

[45] S. Turcotte, S. Larouche, J.N. Beaudry, L. Martinu, R.A. Masut, P. Desjardins, R. Leonelli, Evidence of valence band perturbations in GaAsN/GaAs(001): Combined variable-angle spectroscopic ellipsometry and modulated photoreflectance investigation, Phys. Rev. B - Condens. Matter Mater. Phys. 80 (2009) 85203. doi:10.1103/PhysRevB.80.085203.